15th International Symposium on Ballistics
Jerusalem, Israel, 21-24 May, 1995

HIGH STRAIN RATE PROPERTIES AND CONSTITUTIVE MODELING OF GLASS

Tim J. Holmquist (1), Gordon R. Johnson (1), Dennis E. Grady (2),
Craig M. Lopatin (1) and Eugene S. Hertel Jr. (2)

(1) Alliant Techsystems Inc., 600 2nd St. NE., Hopkins, MN, USA
(2) Sandia National Laboratory, P. O. Box 5800, Albuquerque, NM, USA

This paper presents experimental data and computational modeling for a well-defined glass material. The experimental data cover a wide range of strains, strain rates, and pressures that are obtained from quasi-static compression and tension tests, split Hopkinson pressure bar compression tests, explosively driven flyer plate impact tests, and depth of penetration ballistic tests. The test data are used to obtain constitutive model constants for the improved Johnson-Holmquist (JH-2) brittle material model. The model and constants are then used to perform computations of the various tests.

INTRODUCTION

Recently, much effort has been directed at understanding and modeling brittle materials subjected to impact conditions. Under these conditions brittle materials experience large strains, high strain rates, and high pressures; and under certain conditions may also exhibit bulking or dilatation effects [1]. This paper presents experimental data, for a well-defined glass material, over a wide range of strains, strain rates, and pressures. The data are used to obtain constitutive model constants for the improved Johnson-Holmquist (JH-2) model [2]. The technique used to obtain model constants is discussed and computations of the flyer plate impact and ballistic tests are presented.

TEST DATA

The float glass used for all experiments is the same material that was used for the ballistic penetration tests performed previously [3]. The chemical composition and density are presented in Table 1.

Table 1. Float Glass Chemical Composition and Density

Percent Chemical Composition							Density
SiO_2	Na_2O	CaO	MgO	Al_2O_3	K_2O	Fe_2O_3	(kg/m^3)
73.7	10.6	9.4	3.1	1.8	1.1	0.2	2530

The results of 16 tests performed on the float glass are summarized in Table 2. Tests 1 through 11 are compression and tension tests at two strain rates. These tests were performed on cylindrical specimens where the z-axis is the axis of symmetry. Tests 1 through 4 are quasi-static uniaxial compression tests. Tests 5 through 8 are dynamic compression tests performed using a split Hopkinson pressure bar. Tests 9 through 11 are quasi-static tension tests where the test technique (radial loading) is similar to that used to determine the tensile strength in concrete [4]. For tests 1 through 11 the stress state at failure ($\sigma_x,\sigma_y,\sigma_z,\tau$) is provided, as well as the equivalent stress, σ, pressure, P, and average equivalent strain rate, $\dot{\varepsilon}$.

This work was supported by the United States Department of Energy under Contract DE-AC04-94AL85000.

DISCLAIMER

Table 2. Summary of Test Data for Float Glass

Compression and Tension Tests								
Test Number	Description	σ_x (GPa)	σ_y (GPa)	σ_z (GPa)	τ (GPa)	σ (GPa)	P (GPa)	$\dot{\varepsilon}$ (s^{-1})
1	Compression	0.0	0.0	-1.12	0.0	1.12	0.37	0.001
2	Compression	0.0	0.0	-0.92	0.0	0.92	0.31	0.001
3	Compression	0.0	0.0	-1.17	0.0	1.17	0.39	0.001
4	Compression	0.0	0.0	-0.88	0.0	0.88	0.29	0.001
5	Compression	0.0	0.0	-1.45	0.0	1.45	0.48	250
6	Compression	0.0	0.0	-1.10	0.0	1.10	0.37	250
7	Compression	0.0	0.0	-1.05	0.0	1.05	0.35	250
8	Compression	0.0	0.0	-1.00	0.0	1.00	0.33	250
9	Tension	0.16	-0.48	0.0	0.0	0.42	0.11	0.001
10	Tension	0.17	-0.52	0.0	0.0	0.46	0.12	0.001
11	Tension	0.12	-0.35	0.0	0.0	0.31	0.08	0.001

Flyer Plate Tests								
		HEL			Hugoniot State			
Test Number	Description	σ_z (GPa)	ρ (kg/m^3)	ε_v	σ_z (GPa)	ρ (kg/m^3)	ε_v	$\dot{\varepsilon}$ (s^{-1})
12	Flyer Plate	5.95	2718	-0.069	11.46	3285	-0.230	10^5
13	Flyer Plate	5.95	2718	-0.069	14.25	3408	-0.258	10^5
14	Flyer Plate	5.95	2718	-0.069	18.76	3617	-0.301	10^5

Ballistic Penetration Tests [Anderson et. al. (1993)]				
Test Number	Description	Impact Velocity (m/s)	Penetration, P (mm)	P/L
15	Depth of Penetration	1250	129	1.78
16	Depth of Penetration	1700	172	2.38

Three flyer plate impact experiments were performed (tests 12, 13, and 14) to determine the Hugoniot Elastic Limit (HEL), the Hugoniot stress state, and the particle velocity-time history wave profiles. The volumetric strain is defined as $\varepsilon_v = v/v_0 - 1$ where v and v_0 are the compressed volume and initial volume, respectively. The HEL and Hugoniot states are presented in Table 2 and the wave profiles are presented in Figure 1.

Ballistic penetration experimental results were reported by Anderson et. al. [3]. Tungsten penetrators impacting float glass targets at two velocities were investigated. The final depths of penetration are provided in Table 2.

DETERMINATION OF CONSTANTS FOR THE JH-2 MODEL

The JH-2 model is summarized in Figures 2 and 3. The strength of the material is described by a smoothly varying function of the intact strength, fractured strength, strain rate, and damage. The normalized strength is given by

$$\sigma^* = \sigma^*_i - D(\sigma^*_i - \sigma^*_f) \quad (1)$$

where σ^*_i is the normalized intact strength, σ^*_f is the normalized fractured strength, and D is the damage ($0 \le D \le 1.0$). The normalized equivalent stresses (σ^*, σ^*_i, σ^*_f) have the general form, $\sigma^* = \sigma/\sigma_{HEL}$, where σ is the actual equivalent stress and σ_{HEL} is the equivalent stress at the HEL. The normalized intact strength is given by

$$\sigma^*_i = A(P^* + T^*)^N (1 + C \cdot \ln\dot{\varepsilon}^*) \quad (2)$$

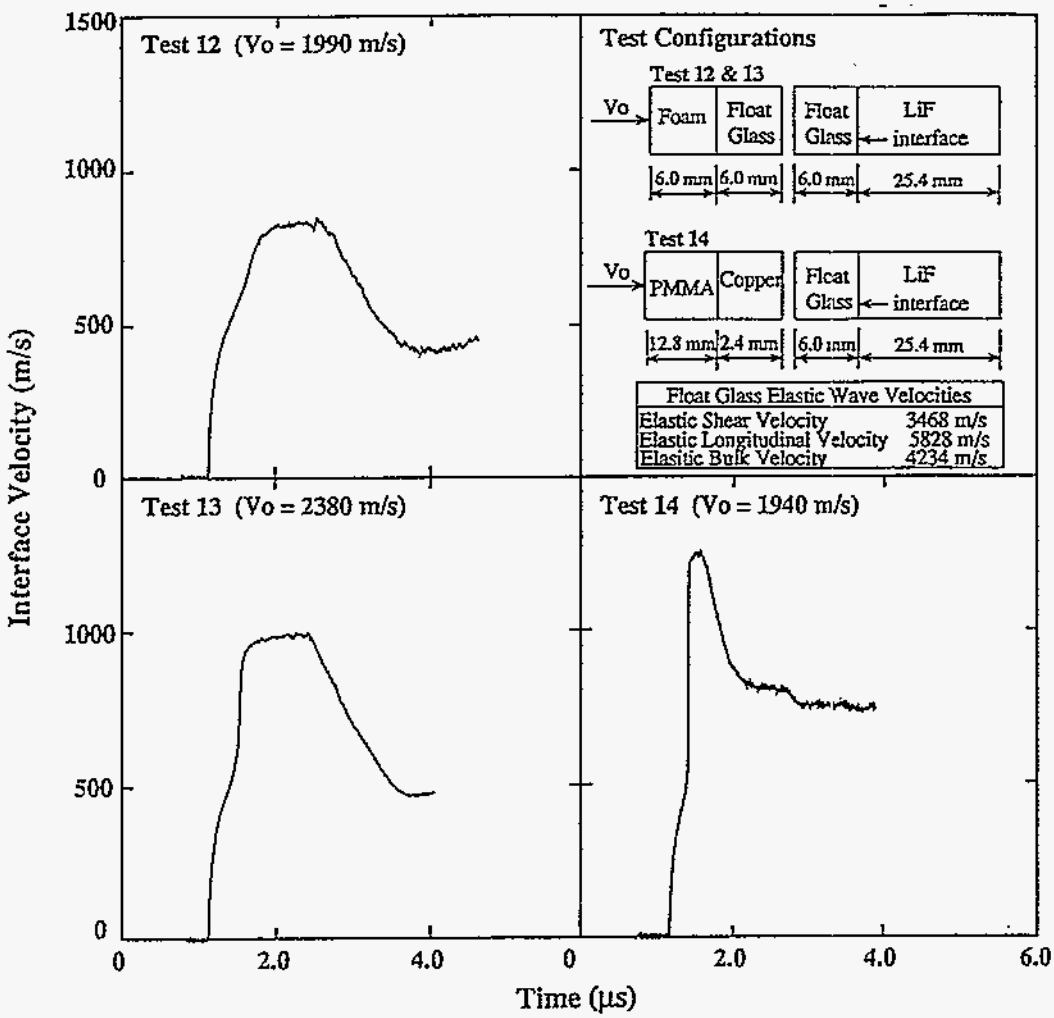

Figure 1. Flyer Plate Impact Tests for Float Glass

and the normalized fractured strength is given by

$$\sigma^*_f = B(P^*)^M (1 + C \bullet \ln\dot{\varepsilon}^*) \tag{3}$$

where the material constants are A, B, C, M, N, and SFMAX. SFMAX is an optional fracture strength parameter that allows the normalized fracture strength to be limited by $\sigma^*_f \leq$ SFMAX. The normalized pressure is $P^* = P/P_{HEL}$, where P is the actual pressure and P_{HEL} is the pressure at the HEL. The normalized maximum tensile hydrostatic pressure is $T^* = T/P_{HEL}$, where T is the maximum tensile hydrostatic pressure the material can withstand. The dimensionless strain rate is $\dot{\varepsilon}^* = \dot{\varepsilon}/\dot{\varepsilon}_0$, where $\dot{\varepsilon}$ is the actual strain rate and $\dot{\varepsilon}_0 = 1.0\ s^{-1}$ is the reference strain rate.

The damage for fracture is accumulated and is given by

$$D = \Sigma\, \Delta\varepsilon_p/\varepsilon_p^f \tag{4}$$

where $\Delta\varepsilon_p$ is the plastic strain during a cycle of integration and $\varepsilon_p^f = f(P)$ is the plastic strain to fracture under a constant pressure, P. The specific expression is given by

$$\varepsilon_p^f = D1(P^* + T^*)^{D2} \tag{5}$$

where D1 and D2 are constants and P* and T* are as defined previously in equation (2).

The hydrostatic pressure is given by

$$P = K1 \bullet \mu + K2 \bullet \mu^2 + K3 \bullet \mu^3 + \Delta P \tag{6}$$

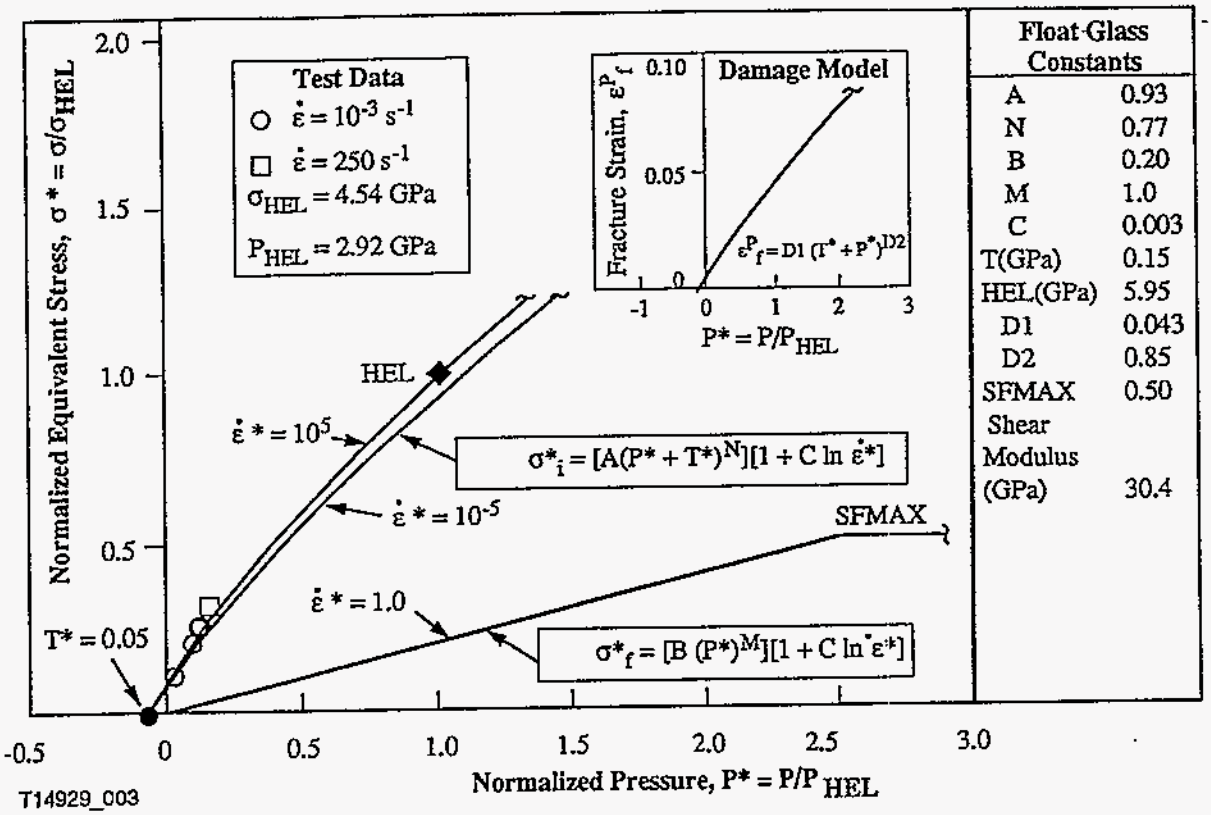

Figure 2. Strength and Damage Model for Float Glass

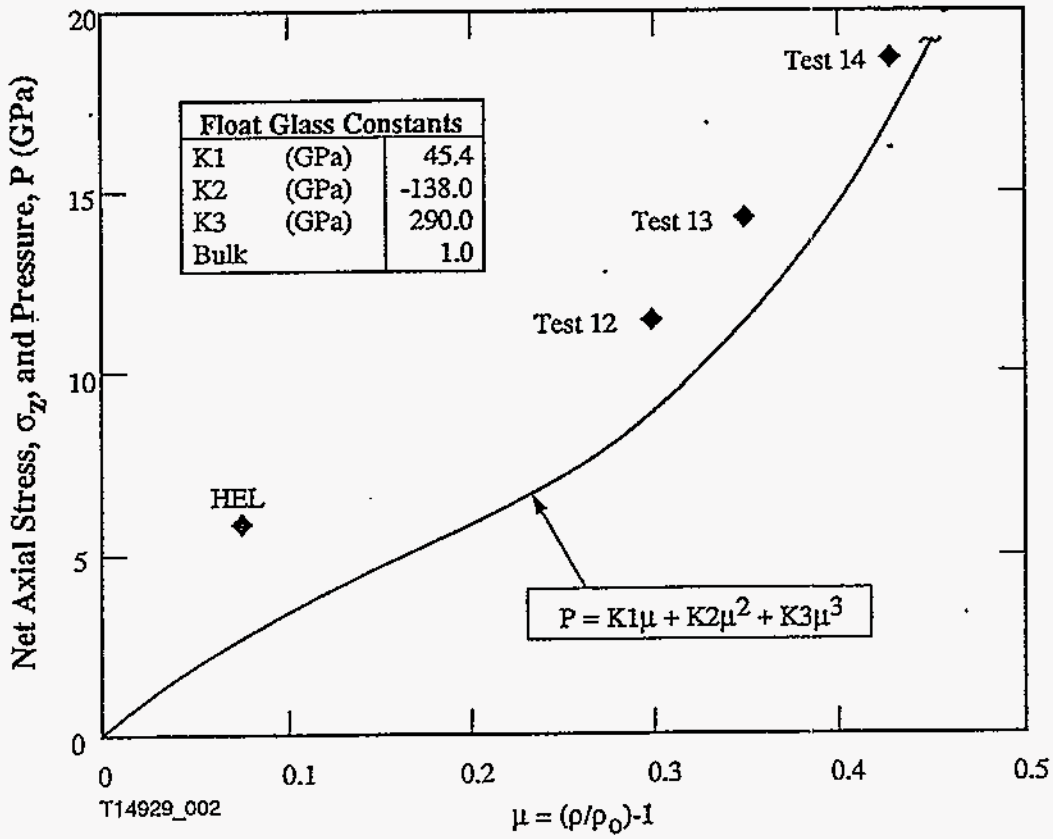

Figure 3. Hydrostat for Float Glass

T14929

where K1, K2, and K3 are constants (K1 is the elastic bulk modulus), and $\mu = \rho/\rho_o - 1$ for current density ρ and initial density ρ_o. After damage begins to accumulate (D>0), bulking can occur by adding an additional incremental pressure ΔP. The pressure increment is determined from energy considerations. The incremental internal elastic energy decrease due to damage is converted to potential internal (hydrostatic) energy by incrementally increasing ΔP. An additional constant, BULK, is the fraction of the elastic energy loss converted to potential hydrostatic energy. When BULK = 1.0, all the internal elastic energy loss is converted to potential hydrostatic energy.

A summary of the constants for float glass is presented in Figures 2 and 3. The strain rate constant, C, provides a measure of the strain rate effect. It influences both the intact and fractured material strength and is determined directly from the test data. C is determined from tension data and uniaxial compression data at two strain rates (tests 1 through 11 from Table 2) and is presented in Figure 4. On the left side of Figure 4 the average uniaxial compressive strength is shown for two strain rates as a function of the pressure. A straight line is drawn from the maximum hydrostatic tensile pressure, T, through each point. The change in slope between the two lines is a measure of the strain rate effect. The change in strength, due to strain rate alone, must be determined at a constant pressure, P. The strength is determined at a constant pressure P = 0.30 GPa. The normalized data are plotted as a function of strain rate on the right side of Figure 4. A straight line is drawn though the data and the strain rate constant C = 0.003 is obtained. The tensile strength, T = 0.015 GPa, is determined by taking the average σ_x from tests 9 through 11.

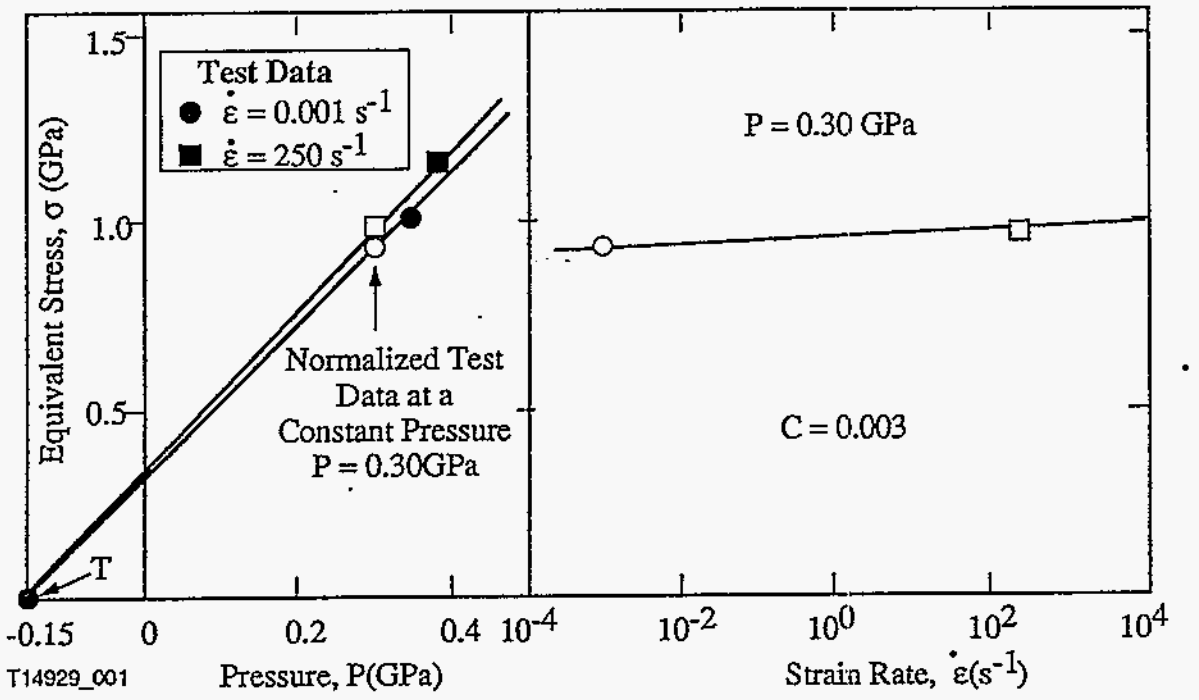

Figure 4. Strain Rate Sensitivity and Constant Determination for Float Glass

Equation 2 describes the intact material strength. It is defined by three constants A, N, and C. The constants A and N are determined by initiating the curve at T*, driving it through the average normalized uniaxial compressive strength (tests 1 through 8) and the normalized HEL equivalent strength at a strain rate $\dot{\varepsilon}^*$=1.0. If the hydrostat of the material is known, the components of pressure, P_{HEL}, and the equivalent strength, σ_{HEL}, can be determined by the relationship HEL = P_{HEL} + (2/3)σ_{HEL}, and constants A and N can be determined explicitly. If the hydrostat is not known, as is the case for float glass, an initial estimate of the pressure at the HEL is made using the relationship $P_{HEL} = K1 \cdot \mu_{HEL}$ where $\mu_{HEL} = \rho_{HEL}/\rho_o - 1.0$ and K1 is the elastic bulk modulus. The initial estimates of A and N are determined from the estimated hydrostat. These constants are finalized after the hydrostat is determined.

The hydrostatic behavior of brittle materials is difficult to obtain directly. Different techniques have been investigated by various researchers, but questions remain as to their validity [5, 6, 7]. Here, a computational iterative technique has been developed to obtain the hydrostat, damage model, and fractured material strength using results from flyer plate impact tests and ballistic tests.

Using the estimated intact material strength determined previously, computations of the flyer plate impact tests and ballistic tests are performed. Various hydrostat constants, damage model constants, and fractured strength constants are investigated. These constants are iterated until the computational results match the test results for both the flyer plate impact tests and the depth of penetration ballistic tests. The resulting hydrostat, damage model and fractured material strength are presented in Figures 2 and 3.

Using this technique, it became apparent that the results for the flyer plate impact computations were most sensitive to the hydrostat, damage model, and SFMAX, while the results for the penetration computations were most sensitive to the fractured material strength below SFMAX. This is probably due to the fact that the average pressures that occur in the flyer plate impact tests are much higher and cover a much larger range than those that occur in the penetration tests.

The hydrostat for float glass, shown in Figure 1, displays an interesting characteristic where the bulk modulus decreases between the HEL and test 12. This behavior is characteristic of glass and is consistent with previous observations [8,9].

Using the defined hydrostat in Figure 1, the components of pressure, P_{HEL} = 2.92 GPa and the equivalent strength, σ_{HEL} = 4.54 GPa at the Hugoniot Elastic Limit (HEL) are determined. These values are used to update the intact material strength constants to obtain A = 0.93 and N = 0.77.

COMPUTATIONAL RESULTS

Computational comparisons to the flyer plate impact tests are presented in Figure 5 and show good correlation. Also shown is the equivalent stress-pressure path that the model produces for test 12. This demonstrates the gradual softening that occurs between points 2 and 3 which produces the dispursed wave front between the HEL and peak Hugoniot stress.

The ballistic test data from Anderson et. al. [3] were simulated to not only provide constant determination, but to investigate the penetration process and the effect of bulking. Figure 6 shows CTH computational results for both ballistic tests. Note that bulking of the float glass tends to close the hole behind the penetrator. Similar results were obtained with the SPH option in the EPIC code.

SUMMARY

Experimental data, on a well-defined glass material, has been presented for a wide range of strains, strain rates, and pressures. The test data were used to obtain constitutive model constants for the Johnson-Holmquist improved (JH-2) brittle material model. The technique used to obtain constants, including computations of the flyer plate impact and ballistic tests, was also presented. The results of the computations show that the model and constants can be used to simulate both wave propagation and penetration. The effect of bulking has also been demonstrated.

ACKNOWLEDGMENTS

The authors would like to thank Dr. Volker Hohler, from the Ernst-Mach-Institut, for providing the float glass material that was used for this work.

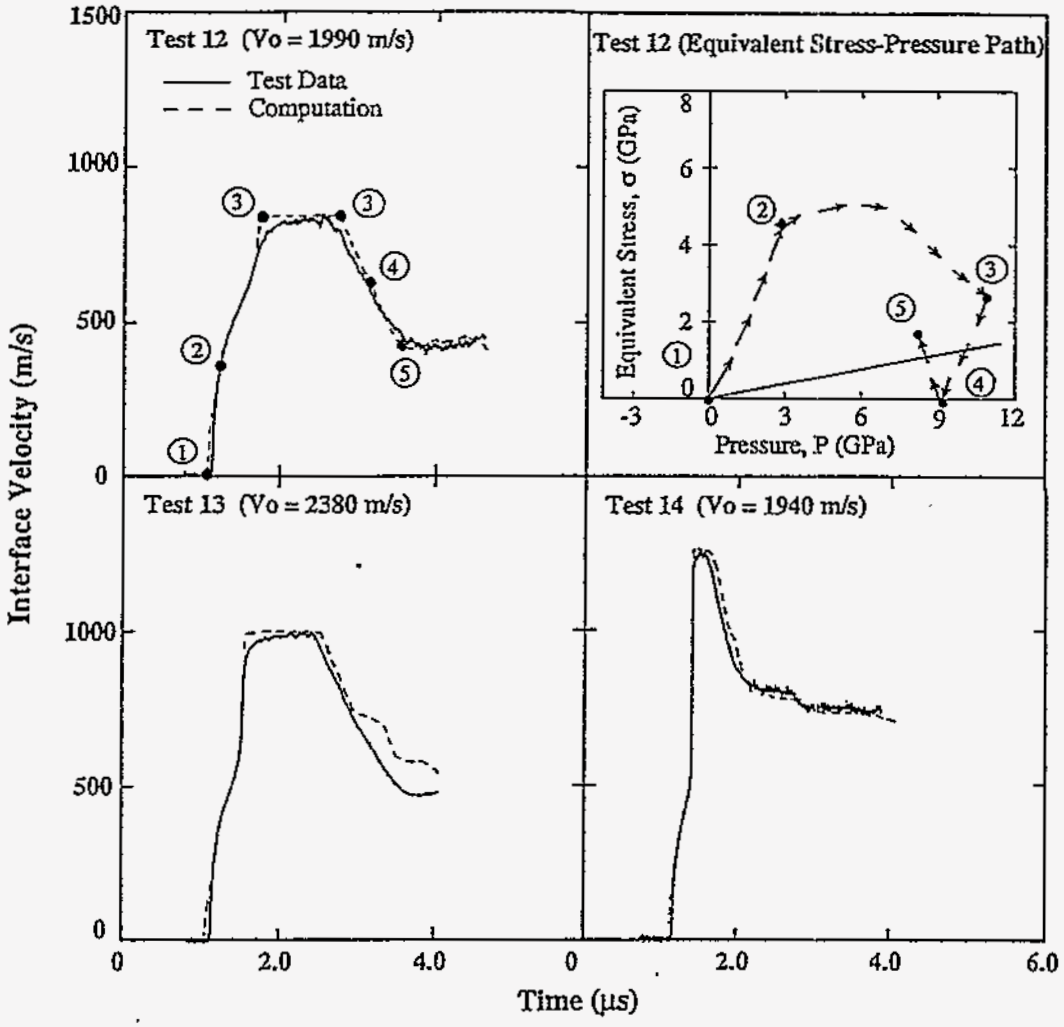

Figure 5. Computational and Test Results for Three Flyer Plate Impact Tests

REFERENCES

[1] G. Holve and J. Cagnoux, "The Behavior of Pyrex Glass Against A Shaped-Charge Jet," Preceedings, Shock Compression of Condensed Matter, 1989. Edited by S.C. Schmidt, J.N. Johnson, and L.W. Davison, Elsevier Science Publishers B.V., 1990.

[2] G.R. Johnson and T.J. Holmquist, "An Improved Computational Constitutive Model for Brittle Materials," *High Pressure Science and Technology*, 1993, AIP Press, 1994.

[3] C.E. Anderson, Jr., V. Hohler, J.D. Walker and A.J. Stilp, "Penetration of Long Rods into Steel and Glass Targets: Experiments and Computations," *Proc. 14th Int. Symp. on Ballistics*, Vol. 1, pp. 145-154, Quebec City, Canada, September 26-29, 1993.

[4] C. Wang and C.G. Salmon, "*Reinforced Concrete Design, 3rd edition*," Harper and Row, New York, 1979.

[5] W.A. Bassett, M.S. Weathers, T.C. Wu and T.J. Holmquist, "Compressibility of SiC up to 68.4 GPa," *Journal of Applied Physics*, Vol. 74, No. 6, pp. 3824-3826, September 15, 1993.

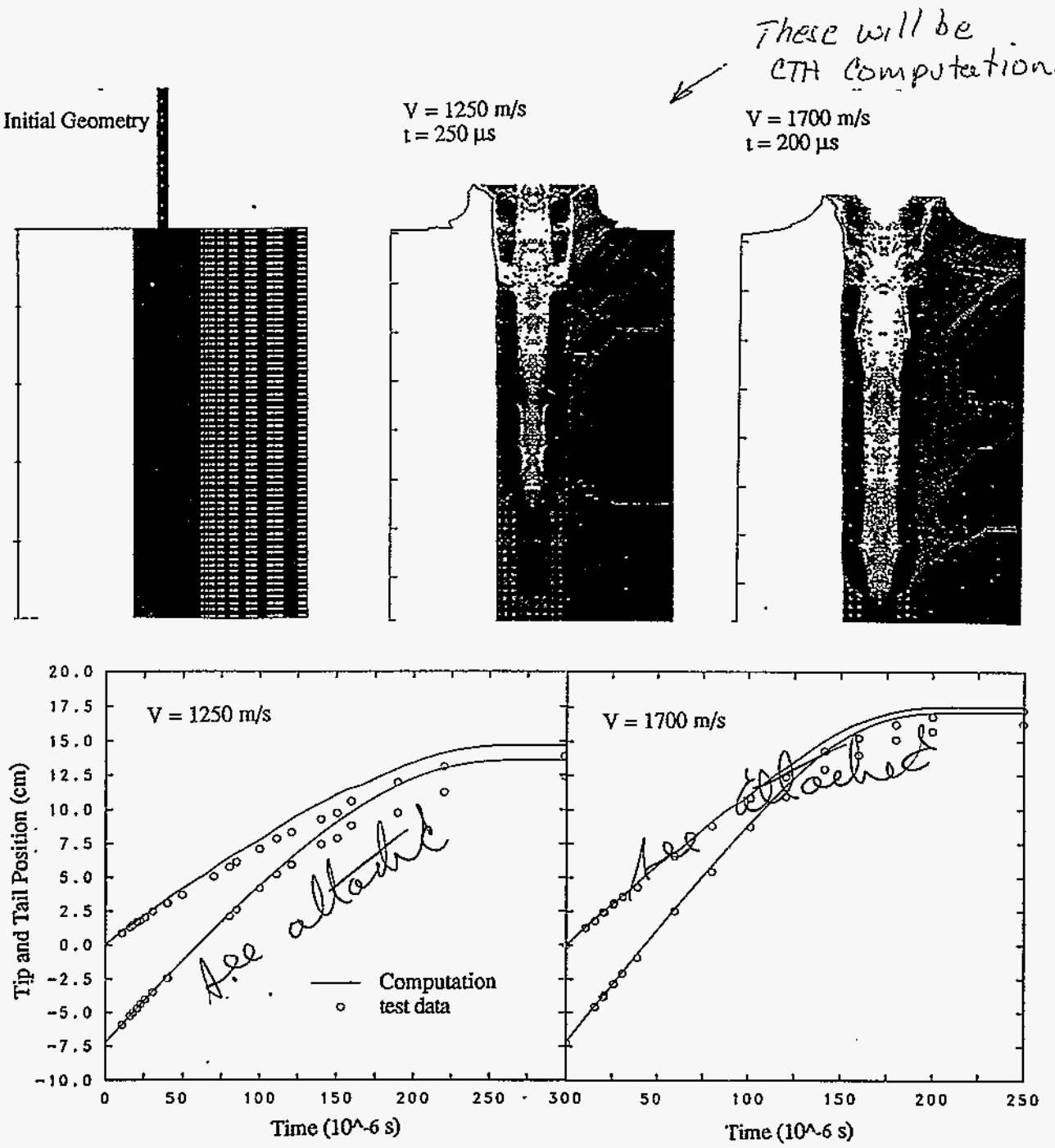

Figure 6. Computational Results for Two Ballistic Tests Using the CTH Code

[6] D.E. Grady, "Hydrodynamic Compressibility of Silicon Carbide through Shock-Compression of Metal-Ceramic Mixtures," *Journal of Applied Physics*, Vol. 75, pp. 197-202, January, 1994.

[7] D.E. Grady, "Shock-Compression and Release Properties of Metal-Ceramic Mixtures," DYMAT, Vol. 1, No. 1, pp. 1-13, March, 1994.

[8] J. Wackerle, "Shock-Wave Compression of Quartz," *Journal of Applied Physics*, Vol. 33, No. 3, March, 1962.

[9] H. Sugiura, K. Kondo and A. Sawaoka, "Dynamic Response of Fuzed Quartz in the Permanent Densification Region," *Journal of Applied Physics*, Vol. 52, May, 1981.

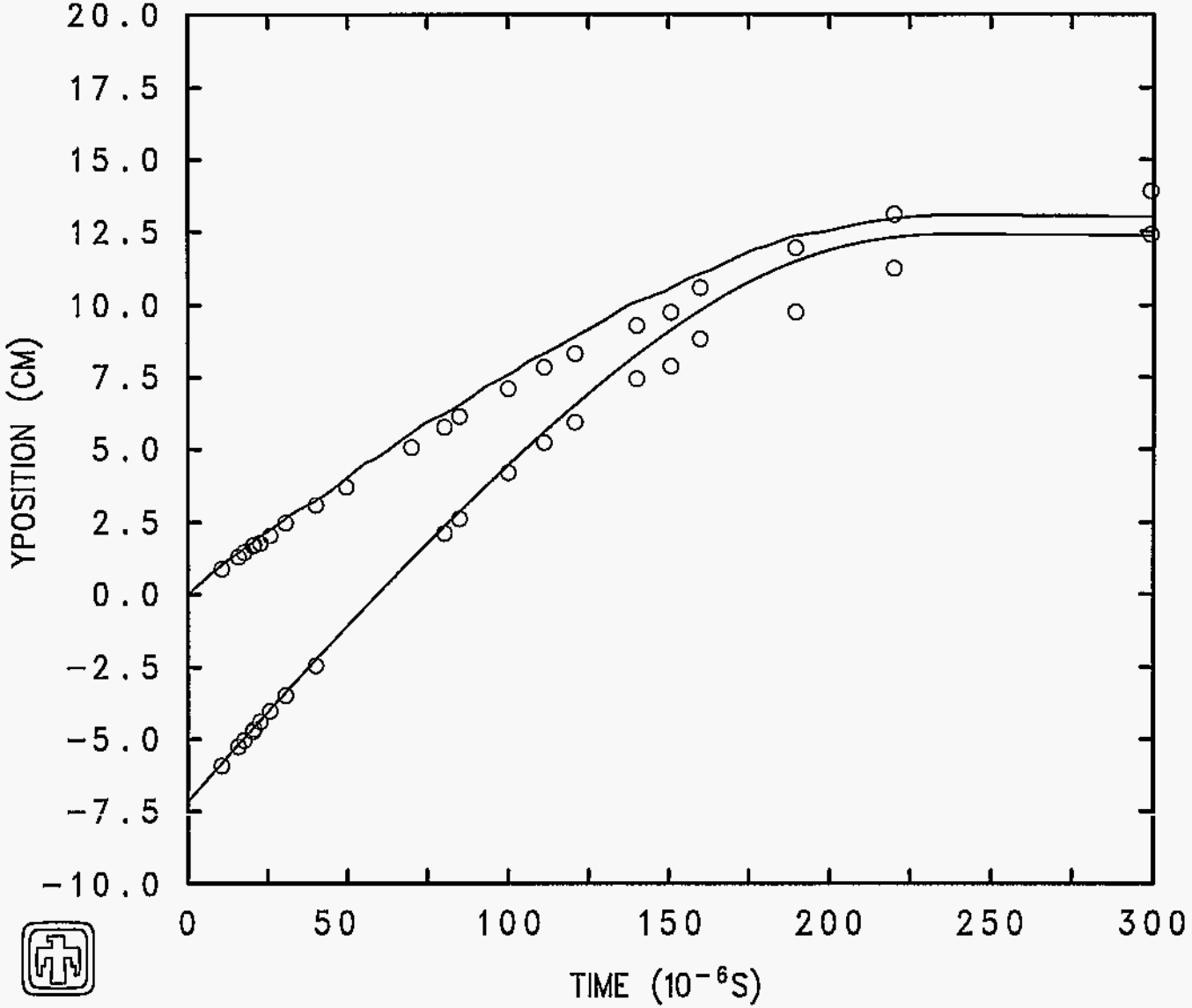

Alliant Test at 1.25 km/s

BCKATP 2/03/95 15:55:17 CTH

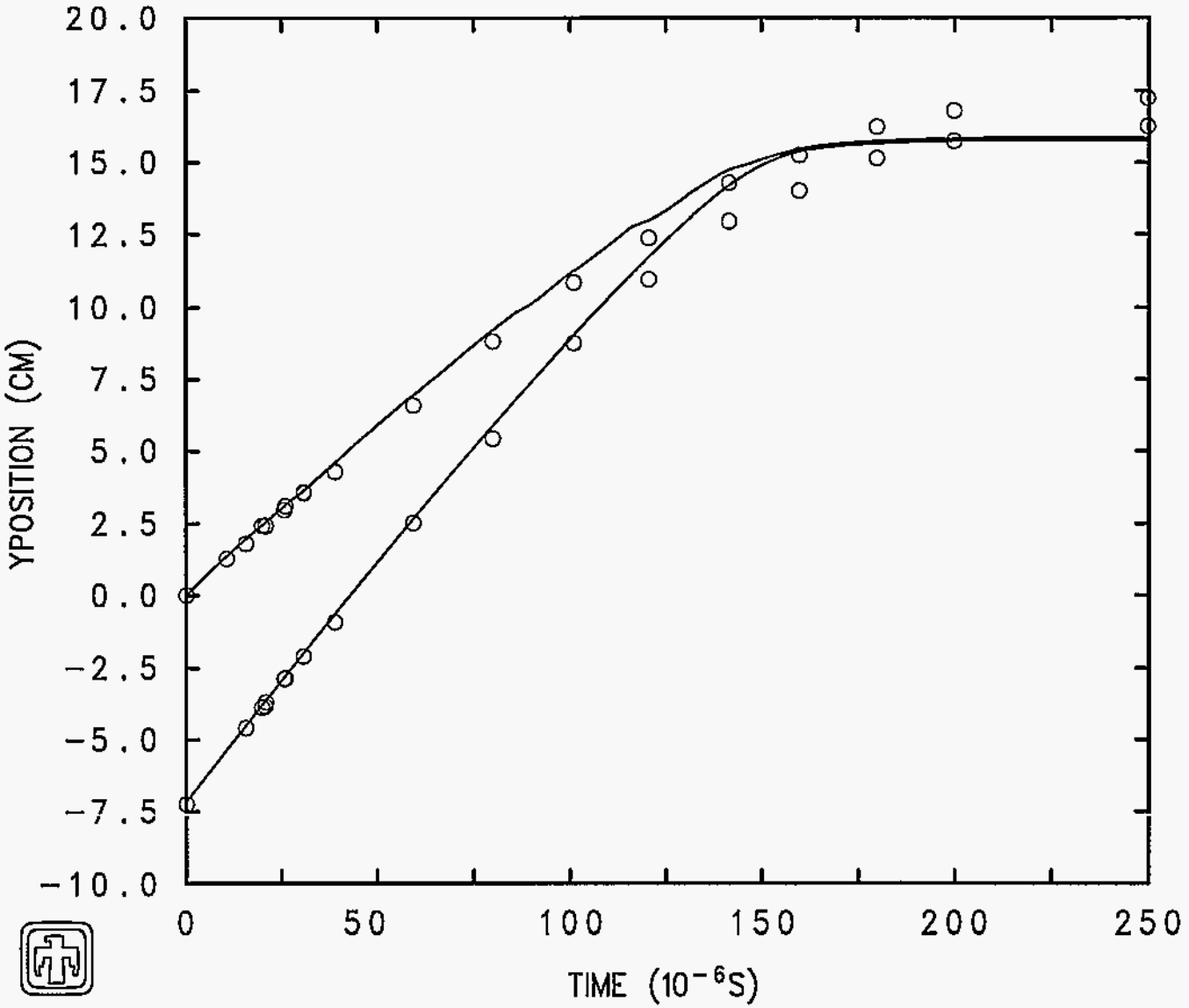

Alliant Test at 1.70 km/s

BBMEGB 2/04/95 04:18:56 CTH

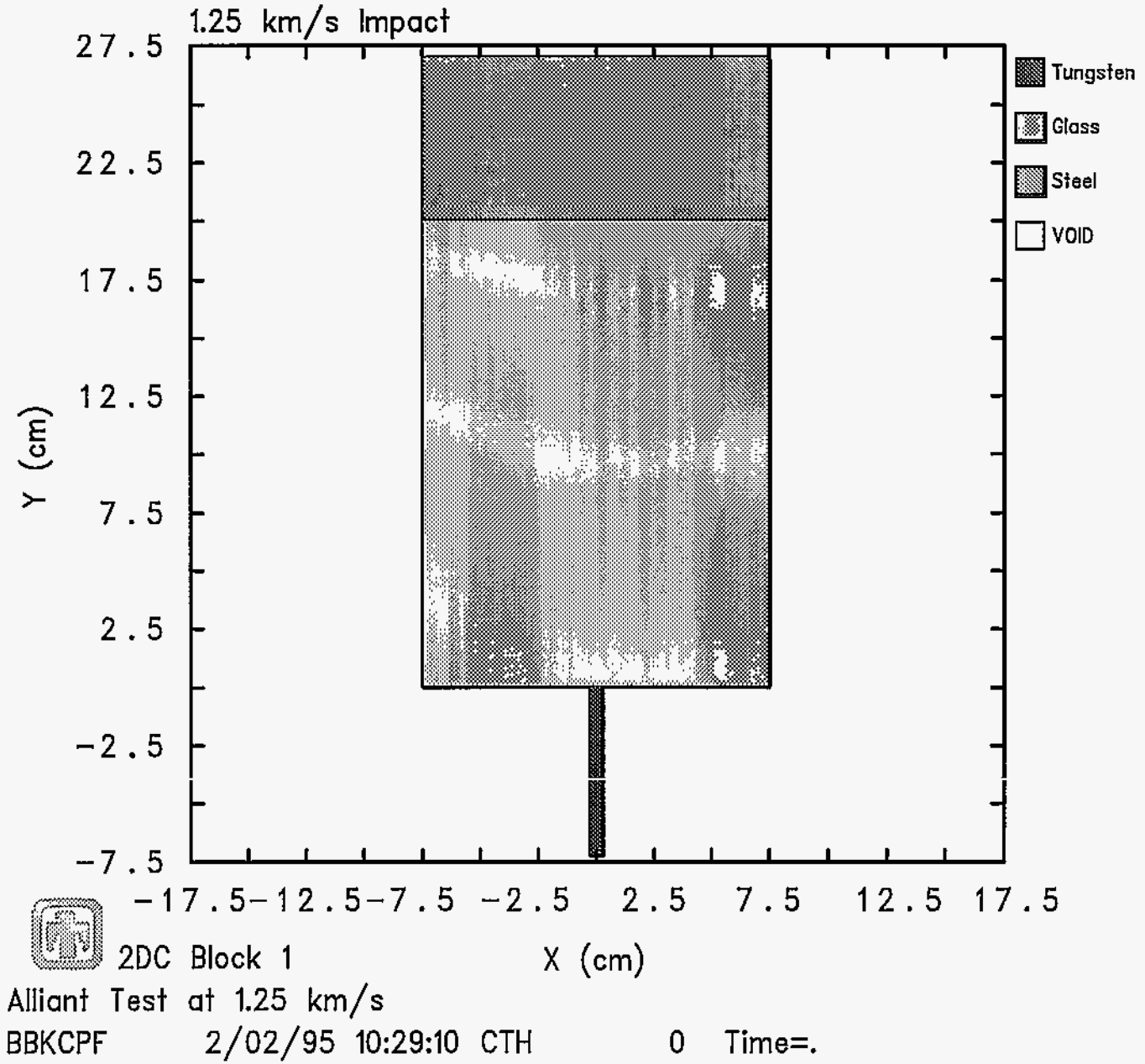
1.25 km/s Impact
27.5
22.5
17.5
12.5
7.5
2.5
-2.5
-7.5
Y (cm)
-17.5 -12.5 -7.5 -2.5 2.5 7.5 12.5 17.5
X (cm)
Tungsten
Glass
Steel
VOID
2DC Block 1
Alliant Test at 1.25 km/s
BBKCPF 2/02/95 10:29:10 CTH 0 Time=.

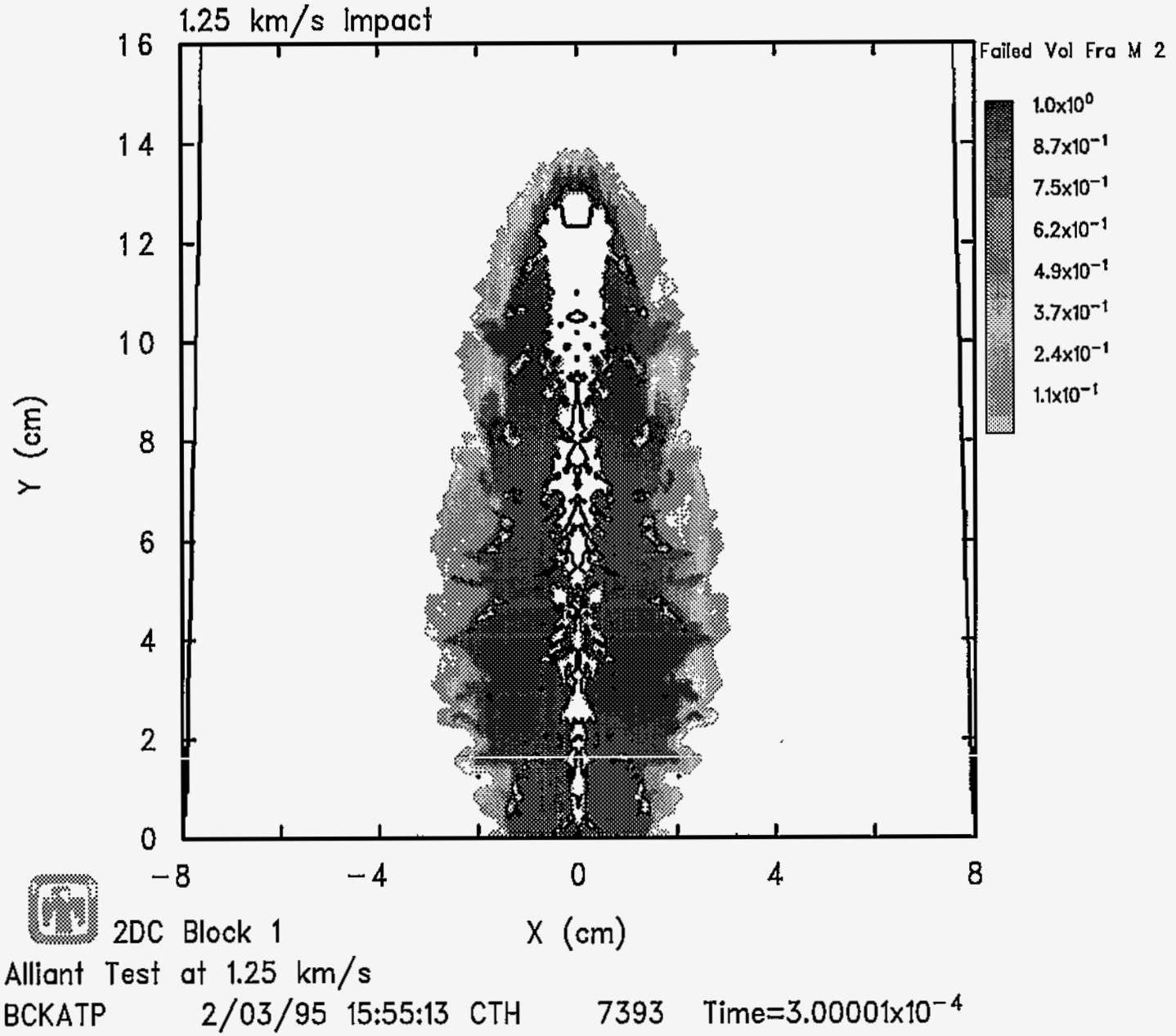
1.25 km/s impact
Failed Vol Fra M 2
1.0x10^0
8.7x10^-1
7.5x10^-1
6.2x10^-1
4.9x10^-1
3.7x10^-1
2.4x10^-1
1.1x10^-1
Y (cm)
X (cm)
16
14
12
10
8
6
4
2
0
-8
-4
0
4
8
2DC Block 1
Alliant Test at 1.25 km/s
BCKATP 2/03/95 15:55:13 CTH 7393 Time=3.00001x10^-4

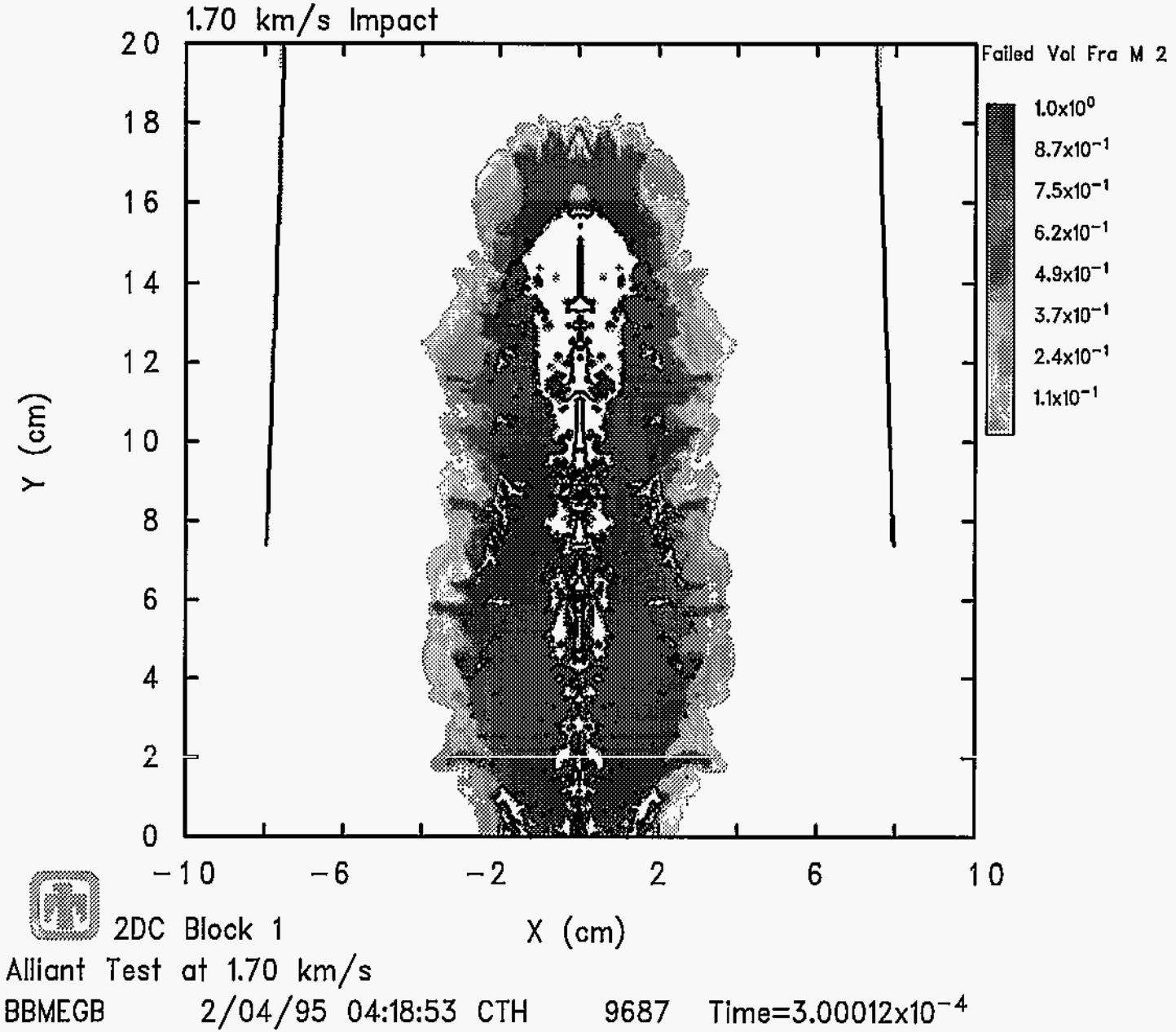
1.70 km/s Impact
Failed Vol Fra M 2
1.0x10^0
8.7x10^-1
7.5x10^-1
6.2x10^-1
4.9x10^-1
3.7x10^-1
2.4x10^-1
1.1x10^-1
Y (cm)
X (cm)
20
18
16
14
12
10
8
6
4
2
0
-10
-6
-2
2
6
10
2DC Block 1
Alliant Test at 1.70 km/s
BBMEGB 2/04/95 04:18:53 CTH 9687 Time=3.00012x10^-4